

Gauge Singlet Scalars as Cold Dark Matter

JOHN McDONALD¹

Cosmology and Astroparticle Physics Group, University of Lancaster, Lancaster LA1 4YB, UK

November 26, 2024

Abstract

In light of recent interest in minimal extensions of the Standard Model and gauge singlet scalar cold dark matter, we provide an arXiv preprint of the paper, published as Phys.Rev. D50 (1994) 3637, which presented the first detailed analysis of gauge singlet scalar cold dark matter.

¹j.mcdonald@lancaster.ac.uk

Abstract

We consider a very simple extension of the standard model in which one or more gauge singlet scalars S_i couples to the standard model via an interaction of the form $\lambda_S S_i^\dagger S_i H^\dagger H$, where H is the standard model Higgs doublet. The thermal relic density of S scalars is calculated as a function of λ_S and the S mass m_S . The regions of the (m_S, λ_S) parameter space which can be probed by present and future experiments to detect scattering of S dark matter particles from Ge nuclei, and to observe upward-moving muons and contained events in neutrino detectors due to high-energy neutrinos from annihilations of S dark matter particles in the Sun and Earth, are discussed. Present experimental bounds place only very weak constraints on the possibility of thermal relic S scalar dark matter. The next generation of cryogenic Ge detectors and of large area (10^4m^2) neutrino detectors will be able to investigate most of the parameter space corresponding to thermal relic S scalar dark matter with $m_S \lesssim 50\text{GeV}$, while a 1 km^2 detector would in general be able to detect thermal relic S scalars with $m_S \lesssim 100\text{GeV}$ as a dark matter candidate and would be able to detect up to $m_S \lesssim 500\text{GeV}$ or more if the Higgs boson is lighter than 100GeV .

1 Introduction

There is strong evidence that the mass density of the Universe is mainly composed of some non-hadronic form of dark matter^[1,2]. Direct observation of galaxies and clusters of galaxies^[2] indicates that $\Omega = 0.1$ to 0.3 , where Ω is the ratio of the mass density to the critical density in the Universe at present. Nucleosynthesis constrains the density of hadronic dark matter to satisfy^[3] $0.011 < \Omega_B h^2 < 0.019$, where $h = 0.5 - 1$ parameterizes the uncertainty in the observed value of the Hubble parameter. Inflation and naturalness considerations^[4] suggest that $\Omega = 1$. Although it seems possible that baryons could just about account for $\Omega = 0.1$ dark matter, it would not be possible for primordial density perturbations to grow sufficiently in a baryon dominated Universe to allow galaxy formation^[5] to be consistent with the magnitude of temperature fluctuations of the cosmic microwave background radiation as observed

by COBE^[6]. This requires the addition of a density of non-hadronic dark matter, preferably cold dark matter (CDM)^[5]. It would also be difficult to explain, if halo dark matter was hadronic in nature, how all the hadrons in galactic halos could be hidden^[7]. Searches for faint stars support the conclusion that the halo dark matter cannot primarily be baryonic^[8] (although recent observations of microlensing by dark objects in the galactic halo do show that at least some baryonic halo dark matter exists^[9]). Thus it is likely that the Universe is dominated by a density of CDM satisfying $\Omega_{\text{CDM}} \gtrsim 0.1$. The age of the Universe imposes an upper limit on Ω , $\Omega h^2 \lesssim 1$ ^[1]. This leaves a window for which a density of particles can consistently serve as the primary component of the halo dark matter, $0.025 \lesssim \Omega h^2 \lesssim 1$.

In this paper we will study in some detail an extremely simple and natural extension of the $SU(3)_c \times SU(2)_L \times U(1)_Y$ standard model, namely, the addition of one or more gauge singlet complex scalars S_i . These scalars, if stable, can in principle account for a density of CDM. Stability of the scalars can most simply be guaranteed if a continuous or discrete symmetry exists under which the gauge singlet scalars are the lightest particles transforming non-trivially. (Additional continuous and discrete symmetries are a common feature of many extensions of the standard model, serving to simplify the models and to eliminate phenomenologically unwelcome interactions such as those leading to baryon and lepton number violation or to flavor-changing neutral currents.) In addition, it is necessary that the S_i do not acquire vacuum expectation values, which in turn requires that they have positive mass squared terms. This model for CDM is essentially determined by just three parameters: the Higgs boson mass m_h , the S scalar mass m_S , and the coupling of the S scalars to the Higgs bosons λ_S . In particular, we will consider the thermal relic density of S scalars, coming from S scalars freezing-out of thermal equilibrium. This is the simplest and most natural origin of a relic density of S scalars, although in principle other possibilities exist, such as S scalars originating in the out-of-equilibrium decay of some heavy particle. We will be particularly interested in the possibility of detecting S scalar cold dark matter, as a function of λ_S , m_S and m_h , either via direct detection of the recoil energy coming from elastic scattering of S dark matter particles from Ge nuclei^[10,11], or by observing upward moving muons

or contained events in neutrino detectors, produced by high-energy neutrinos coming from S annihilations in the Sun or in the Earth^[12–17].

The paper is organized as follows. In section 2 we discuss the thermal relic density of gauge singlet scalars in the Universe at present. In section 3 we discuss the elastic scattering of S scalars from Ge nuclei. In section 4 we discuss the rate of upward moving muons and contained events produced by high energy neutrinos due to S annihilations in the core of the Sun and of the Earth. In section 5 we give our conclusions. In the Appendix we give some details of the calculation of the upward-moving muon and contained event rates.

2 S scalar dark matter

We consider extending the standard model by the addition of terms involving the S scalars

$$L_S = \partial^\mu S_i^\dagger \partial_\mu S_i - m^2 S_i^\dagger S_i - \lambda_S S_i^\dagger S_i H^\dagger H \quad (2.1),$$

where $i = 1, \dots, N$. This model has a global U(1) symmetry, $S_i \rightarrow e^{i\alpha} S_i$, which guarantees the stability of the S_i scalars by eliminating the interaction terms involving odd powers of S_i and S_i^\dagger which lead to S_i decay. We first consider the case $N = 1$. In order to calculate the relic density arising from S scalars freezing out of thermal equilibrium we will use the usual Lee-Weinberg (LW) approximation^[18] to solve the rate equation for the density of S_i scalars. The rate equation is given by

$$\frac{dn_S}{dt} = -3Hn_S - \langle \sigma_{\text{ann}} v_{\text{rel}} \rangle (n_S^2 - n_o^2) \quad (2.2).$$

σ_{ann} is the SS^\dagger annihilation cross-section, v_{rel} is the relative velocity of the annihilating particles and H is the expansion rate of the Universe. The angular brackets denote the thermal average value. (2.2) gives the number density of S scalars n_S . The total density of S and S^\dagger scalars is then $2n_S$. The equilibrium S density n_o , for $m_S/T \gg 1$, is given by

$$n_o = T^3 \left(\frac{m_S}{2\pi T} \right)^{3/2} e^{-\frac{m_S}{T}} \quad (2.3).$$

The approximate solution of (2.2) is then found by rewriting (2.2) as

$$\frac{df}{dT} = \frac{\langle \sigma_{\text{ann}} v_{\text{rel}} \rangle}{K} (f^2 - f_o^2) \quad (2.4),$$

where $f = \frac{n_S}{T^3}$, $f_o = \frac{n_o}{T^3}$ and $K = (4\pi^3 \bar{g}(T)/45M_{\text{Pl}}^2)^{1/2}$. $\bar{g}(T)$ is the number of degrees of freedom with masses smaller than T . In this we are assuming that the number of degrees of freedom in thermal equilibrium with the photons, $g(T)$, is constant around the S freeze-out temperature T_{fS} , i.e. no particle thresholds at $T \approx T_{\text{fS}}$, and also that the Universe is radiation dominated. The LW solution is given by assuming that $f = f_o$ until the temperature at which

$$\left| \frac{df_o}{dT} \right| = \frac{\langle \sigma_{\text{ann}} v_{\text{rel}} \rangle}{K} f_o^2 \quad (2.5)$$

is satisfied, which defines the S freeze-out temperature, T_{fS} . Then for $T < T_{\text{fS}}$ one solves (2.4) with $f_o = 0$ on the right hand side and with $f(T_{\text{fS}}) = f_o(T_{\text{fS}})$. The freeze-out temperature is then obtained from

$$x_{\text{fS}}^{-1} = \ln \left(\frac{m_S x_{\text{fS}}^2 A}{(1 - 3x_{\text{fS}}/2) (2\pi x_{\text{fS}})^{3/2}} \right) \quad (2.6),$$

where $x_{\text{fS}} = T_{\text{fS}}/m_S$ and $A = \frac{\langle \sigma_{\text{ann}} v_{\text{rel}} \rangle}{K}$. The present total mass density in S scalars and antiscalars is then

$$\Omega_S \equiv \frac{\rho_S + \rho_{S^\dagger}}{\rho_c} = 2 \frac{g(T_\gamma)}{g(T_{\text{fS}})} \frac{K}{T_\gamma x_{\text{fS}} \langle \sigma_{\text{ann}} v_{\text{rel}} \rangle} \left(\frac{T_\gamma^4}{\rho_c} \right) \frac{(1 - 3x_{\text{fS}}/2)}{(1 - x_{\text{fS}}/2)} \quad (2.7),$$

where it has been assumed that $\langle \sigma_{\text{ann}} v_{\text{rel}} \rangle$ is T independent. $\rho_c = 7.5 \times 10^{-47} h^2 \text{GeV}^4$ is the critical closure density of the Universe at present ($h = 0.5$ to 1) and T_γ is the present photon temperature.

In order to calculate $\langle \sigma_{\text{ann}} v_{\text{rel}} \rangle$ we need the SS^\dagger annihilation modes. These are shown in Figure 1. The corresponding contributions to $\langle \sigma_{\text{ann}} v_{\text{rel}} \rangle$ are given by

$SS^\dagger \rightarrow h^o h^o$:

$$\frac{\lambda_S^2}{64\pi m_S^2} \left(1 - \frac{m_h^2}{m_S^2} \right)^{1/2} \quad (2.8a),$$

$SS^\dagger \rightarrow W^+ W^-$:

$$2 \left(1 + \frac{1}{2} \left(1 - \frac{2m_S^2}{m_W^2} \right)^2 \right) \frac{\lambda_S^2 m_W^4}{8\pi m_S^2 \left((4m_S^2 - m_h^2)^2 + m_h^2 \Gamma_h^2 \right)} \left(1 - \frac{m_W^2}{m_S^2} \right)^{1/2} \quad (2.8b),$$

SS[†] → Z⁰Z⁰ :

$$2 \left(1 + \frac{1}{2} \left(1 - \frac{2m_S^2}{m_Z^2} \right)^2 \right) \frac{\lambda_S^2 m_Z^4}{16\pi m_S^2 \left((4m_S^2 - m_h^2)^2 + m_h^2 \Gamma_h^2 \right)} \left(1 - \frac{m_Z^2}{m_S^2} \right)^{1/2} \quad (2.8c),$$

SS[†] → $\bar{f}f$:

$$\frac{m_W^2}{\pi g^2} \frac{\lambda_f^2 \lambda_S^2}{\left((4m_S^2 - m_h^2)^2 + m_h^2 \Gamma_h^2 \right)} \left(1 - \frac{m_f^2}{m_S^2} \right)^{3/2} \quad (2.8d).$$

Here the fermion Yukawa coupling is $\lambda_f = m_f/v$ where $v = 250\text{GeV}$ and m_f is the fermion mass. m_h is the Higgs boson mass, and Γ_h is the Higgs decay width, for which we use the standard model values^[19]. We should note that the assumption made in arriving at (2.7), that $\langle \sigma_{\text{ann}} v_{\text{rel}} \rangle$ is T independent, is strictly true only for freeze-out temperatures small compared with the electroweak phase transition temperature T_{EW} , where^[20]

$$T_{\text{EW}} = \frac{2.4m_h}{\left(1 + 0.62 \left(\frac{m_t}{m_W} \right)^2 \right)^{1/2}} \quad (2.9),$$

and m_t is the t quark mass. The thermal expectation value of the Higgs field is given by $\langle h^0 \rangle_T = v \left(1 - \frac{T^2}{T_{\text{EW}}^2} \right)^{1/2}$. Thus for $T_{\text{fs}} \gtrsim T_{\text{EW}}$ the effective mass of the W and Z bosons goes to zero, while the $\langle h^0 \rangle_T$ dependent S and h^0 masses differ from their zero temperature values. In practice, however, $T_{\text{fs}} \gtrsim T_{\text{EW}}$ occurs only for very large S masses $\gtrsim 1\text{TeV}$. In this limit, the S mass is essentially determined by the constant mass term m in (2.1) and so is effectively $\langle h^0 \rangle$ independent, while from (2.8b) and (2.8c), in the limit $m_S \gg m_W$ and $m_S \gg m_h/2$ the contribution from S annihilations to W and Z bosons reduces to 3 times the contribution from annihilations to the Higgs boson (2.8a), as expected in the SU(2) \times U(1) symmetric limit. This is T independent. A large Higgs boson mass doesn't alter this conclusion, since from (2.9) T_{EW} is of order the Higgs mass, and so if T_{fs} is of order T_{EW} , then m_S , which, as discussed below, is much larger than T_{fs} , will also be much larger than m_h . As a result, we can neglect m_h in the propagators of (2.8). Thus in practice we can use the cross-sections (2.8) calculated with the T=0 value for $\langle h^0 \rangle$, $\langle h^0 \rangle = 250\text{GeV}$.

Using these contributions to $\langle \sigma_{\text{ann}} v_{\text{rel}} \rangle$ we solve (2.6) self-consistently for the freeze-out temperature and then obtain from (2.7) the resulting dark matter density.

In Figures 2(a)-2(d) we give plots of the dark matter density as a function of m_S and λ_S for various values of m_h . In these we show the contours for $\Omega_S h^2 = 1.0$, corresponding to the upper limit from the age of the Universe, $\Omega_S h^2 = 0.25$, which is the smallest value for which a critical density ($\Omega_S = 1$) of S scalars can occur, and $\Omega_S h^2 = 0.025$, corresponding to the smallest value for which S dark matter could make up the primary component of the galactic halo. In Table 1 we give values of the freeze-out temperature for various values of λ_S , m_S and m_h . Typically $m_S = (10 - 30)T_{\text{fs}}$ for the range of parameters we are considering. We have assumed $m_t = 120\text{GeV}$ throughout. We find that increasing the t quark mass to 200GeV makes only a very small difference to the results.

Table 1. S freeze-out temperature, $x_{\text{fs}}^{-1} = m_S/T_{\text{fs}}$

λ_S	m_S	m_h	x_{fS}^{-1}	λ_S	m_S	m_h	x_{fS}^{-1}
1	30	60	34.5	0.01	30	60	25.5
1	30	100	23.5	0.01	30	100	14.6
1	30	300	18.5	0.01	30	300	9.6
1	30	500	16.5	0.01	30	500	7.7
1	100	60	27.9	0.01	100	60	18.9
1	100	100	28.3	0.01	100	100	19.3
1	100	300	26.5	0.01	100	300	17.5
1	100	500	23.9	0.01	100	500	14.9
1	1000	60	25.1	0.01	1000	60	16.1
1	1000	100	25.1	0.01	1000	100	16.1
1	1000	300	25.1	0.01	1000	300	16.1
1	1000	500	25.2	0.01	1000	500	16.2

From Figures 2(a)-2(d) we see that for large values of λ_S (larger than 0.1), which is particularly interesting from the point of view of the phenomenology of S scalars, in order to have a density of S scalars which can account for a critical density of dark matter ($\Omega_S h^2 \gtrsim 0.25$), we require the S mass typically to be $\lesssim 100\text{GeV}$ or $\gtrsim 500\text{GeV}$. More generally, as the Higgs boson mass increases, the value of λ_S for which S particles of mass less than about 100GeV can account for dark matter increases, from about

$\lambda_S = 0.01 - 0.1$ for $m_h = 60\text{GeV}$ to $\lambda_S \gtrsim 1$ for $m_h \gtrsim 300\text{GeV}$. This could be important with respect to the possibility of producing S particles via Higgs decay at future multi-TeV hadron colliders such as the CERN Large Hadron Collider (LHC) [19].

These results are for the case $N=1$. If we consider several scalars of equal mass and coupling strength to the Higgs (for example, if the S_i were a multiplet under a global symmetry or even gauge symmetry with a symmetry breaking scale large compared with m_W), then it is easy to see that the total density in S_i and S_i^\dagger is just the sum over each individual S_i density, since each S_i annihilates only with its own antiparticle. Thus

$$\Omega_{S \text{ Total}} \equiv \sum_i \Omega_{S_i} = N\Omega_S \quad (2.10)$$

Since $\Omega_S \propto \frac{1}{\langle \sigma_{\text{ann}} v_{\text{rel}} \rangle} \propto \frac{1}{\lambda_S^2}$, we see that Figure 2 still holds if we replace λ_S by $\hat{\lambda}_S = \lambda_S/\sqrt{N}$ on the horizontal axis. Thus for a given value of Ω_S and m_S the value of λ_S is increased by \sqrt{N} . This will increase strength of interaction with matter and so the observability of S dark matter for $N > 1$.

3 Elastic scattering of S dark matter particles from nuclei and constraints from Ge detectors.

In this section we consider the constraints on λ_S and m_S following from direct detection of S dark matter particles via elastic scattering of S scalars from Ge nuclei[10,11]. It will be assumed throughout that S dark matter accounts for the halo dark matter density. Although the simplest possibility for the origin of a relic density of S particles is from S freeze-out, in principle there are other possibilities. For example, if a heavy particle such as a heavy right-handed neutrino N decays to S particles (via the Higgs-mediated process $N \rightarrow \nu_L S^\dagger S$ in the case of right-handed neutrinos) at a temperature below the S freeze-out temperature (typically between 1GeV and 50GeV for $20\text{GeV} \lesssim m_S \lesssim 1000\text{GeV}$) then the S particles so produced will not return to an equilibrium density and will result in a relic S density different from the thermal relic density. In this case halo dark matter could, in principle, be accounted for by any combination of m_S and λ_S . Thus it is important to consider generally what constraints on

the parameters of the model are imposed by experimental observations, as well as to compare the constraints with the thermal relic density as a particular example.

The S scattering cross-section from quarks via Higgs exchange gives an effective interaction

$$L_{\text{eff}} = \frac{\lambda_S m_q}{m_h^2} S^\dagger S \bar{q} q \quad (3.1).$$

Using the expression for the nuclear matrix element^[16,21]

$$\langle N | \Sigma_q m_q \bar{q} q | N \rangle = (7.62) \frac{2}{27} m_N \bar{\psi}_N \psi_N ,$$

we see that the effective interaction with a nucleus is given by

$$L_{\text{eff}} = (7.62) \frac{2}{27} \frac{\lambda_S m_N}{m_h^2} S^\dagger S \bar{\psi}_N \psi_N \quad (3.2)$$

and that the cross-section for coherent S-nucleus scattering is given by

$$\sigma_{S-N} = (7.62)^2 \frac{1}{(27\pi)^2} \frac{\pi m_N^4}{(m_S + m_N)^2} \frac{\lambda_S^2}{m_h^4} \quad (3.3).$$

In general σ_{S-N} must be multiplied by a correction factor $\zeta_N(m_S)$, which accounts for the fact that at large enough momentum transfer the scattering ceases to be a coherent scattering with the whole nucleus^[14]. We will use a correction factor based on integrating a Gaussian nuclear form factor over the Maxwellian velocity distribution of the halo dark matter particles^[14,22]:

$$\zeta_N(m_S) = \frac{0.573}{b} \left[1 - \frac{\exp(-\frac{b}{(1+b)}) \operatorname{erf}(\sqrt{\frac{1}{1+b}})}{\sqrt{(1+b)} \operatorname{erf}(1)} \right] \quad (3.4),$$

where

$$b = \frac{8}{9} \bar{v}^2 r_{\text{charge}}^2 \frac{m_S^2 m_N^2}{(m_S + m_N)^2} , \quad (3.5)$$

$$r_{\text{charge}} = 5.1(0.3 + 0.89A^{1/3}) \text{GeV}^{-1} ,$$

and $\bar{v} = v_{300} 300 \text{kms}^{-1}$ is the mean halo velocity dispersion of the S particles, which is related to the galactic rotation velocity in the isothermal sphere model, v_{rot} , by $\bar{v} = \sqrt{3/2} v_{\text{rot}}$. For the case of scattering from Ge we find that the full cross-section is given by

$$\sigma_{S-\text{Ge}} = 5.7 \times 10^{-36} \text{cm}^{-2} \frac{\zeta_N(m_S)}{\left(1 + \frac{m_S}{76 \text{GeV}}\right)^2} \left(\frac{100 \text{GeV}}{m_h}\right)^4 \left(\frac{\lambda_S}{0.1}\right)^2 \quad (3.6),$$

where $\zeta_N(m_S)$ is given by (3.4) with

$$b = 2.2v_{300}^2/(1 + 76\text{GeV}/m_S)^2 .$$

In order to compare with experiments we need the rate of interaction of the halo dark matter particles with a detector per kg per day. This is given by (without energy threshold)^[23]

$$R = \left(\frac{8}{3\pi}\right)^{1/2} \frac{\eta_v \bar{v} \rho_h \sigma_{S-N} \eta_N(m_S)}{m_S m_N} = 0.069 \rho_{0.4} v_{300} \sigma_{36}^N \left(\frac{100\text{GeV}}{m_N}\right) \left(\frac{100\text{GeV}}{m_S}\right) \text{kg}^{-1} \text{d}^{-1} \quad (3.7),$$

where $\rho_{0.4}$ is the density of S scalars in the halo (ρ_h) in units of 0.4GeV cm^{-3} , $\eta_v \approx 1.3$ is a correction for the motion of the Sun and the Earth, and σ_{36}^N is the corrected S-N cross-section in units of 10^{-36}cm^2 .

It should be noted that the correction factor $\zeta_N(m_S)$ is not accurate for dark matter particle masses much larger than 100GeV ^[22]. However, we will see that the experimental constraints in the present model are most important for S masses less than about 100GeV , in which case the correction factor (3.4) is accurate to about 10% ^[22].

In Figure 3 we show the event rate as a function of m_S and λ_S for the cases $m_h = 60\text{GeV}$, 100GeV and 300GeV . We also show the contours corresponding to the thermal relic S dark matter region of the parameter space, $0.025 \lesssim \Omega_S \lesssim 1$. (We have assumed $\rho_{0.4} = v_{300} = 1$ throughout).

The present experimental upper bound on R corresponds approximately to $100\text{kg}^{-1}\text{d}^{-1}$ for $m_S \gtrsim 10\text{GeV}$ ^[10,11,24]. In general, present ionization detectors may be able to achieve a sensitivity of about $10\text{kg}^{-1}\text{d}^{-1}$ ^[24], while in the future cryogenic Ge detectors (such as a proposed $500\text{g}^{73}\text{Ge} + 500\text{g}^{76}\text{Ge}$ detector^[25]) should be able to achieve a sensitivity of $0.1\text{kg}^{-1}\text{d}^{-1}$. We see from Figure 3 that in order to constrain the thermal relic S region of parameter space we need an upper bound on R which is less than $100\text{kg}^{-1}\text{d}^{-1}$. For an upper bound on the cross-section of $10\text{kg}^{-1}\text{d}^{-1}$, we can probe a small region of the thermal relic parameter space corresponding to $\lambda_S \gtrsim 0.06$ and $m_S \lesssim 20\text{GeV}$. In order to significantly constrain the possibility of a critical density of S dark matter, $0.25 \lesssim \Omega_S h^2 \lesssim 1.0$, we require $R \lesssim 1\text{kg}^{-1}\text{d}^{-1}$. $R \lesssim 0.1\text{kg}^{-1}\text{d}^{-1}$ would allow us to detect or exclude almost all thermal relic S dark matter for $m_S \lesssim 50\text{GeV}$, while

$R \lesssim 0.01\text{kg}^{-1}\text{d}^{-1}$ would detect almost all thermal relic S dark matter for $m_S \lesssim 100\text{GeV}$. These conclusions for $m_S \lesssim 100\text{GeV}$ are essentially independent of m_h , as can be seen by comparing Figures 3(a), 3(b) and 3(c). For $m_S \gtrsim 100\text{GeV}$, the amount of thermal relic parameter space which can be experimentally searched decreases as m_h increases. From Figure 3(a) we see that even with m_h as small as 60GeV , in order to constrain the thermal relic dark matter for $m_S \gtrsim 100\text{GeV}$ we would need $R \lesssim 0.01\text{kg}^{-1}\text{d}^{-1}$, and even if an upper bound as low as $0.01\text{kg}^{-1}\text{d}^{-1}$ could be achieved, this would not be sufficient to constrain the possibility of a critical density of thermal relic S dark matter for $m_S \gtrsim 100\text{GeV}$.

Thus we can conclude that since present Ge ionization detectors give an upper bound on R of about $100\text{kg}^{-1}\text{d}^{-1}$ (and are not expected achieve a sensitivity better than $10\text{kg}^{-1}\text{d}^{-1}$), present attempts at direct detection of dark matter can at best only impose a very weak constraint on the possibility of thermal relic S dark matter. The next generation of cryogenic detectors should be able to effectively search for S dark matter up to at least 50GeV . Thermal relic S scalars significantly heavier than 100GeV are probably beyond the reach of future Ge detectors, even if the Higgs mass is as small as 60GeV .

4 High energy neutrinos from SS^\dagger annihilation in the Earth and the Sun.

In this section we calculate the flux of upward-moving muons and the rate of contained events in neutrino detectors due to high-energy neutrinos ($> 2\text{GeV}$) resulting from annihilations of SS^\dagger pairs in the core of the Earth and the Sun^[12–17].

The rate of upward-moving muons at the surface of the Earth due to annihilations in the Sun is given by ^[13]

$$\Gamma_{\text{detector}} = 1.27 \times 10^{-29} C m_S^2 \sum_i a_i b_i \Sigma_F B_F \langle N z^2 \rangle_{F i} \text{m}^{-2} \text{yr}^{-1} \quad (4.1),$$

where C is the capture rate in the Sun in units s^{-1} , a_i and b_i are the neutrino-scattering and muon-range coefficients, summed over $i = \nu_\mu$ and $\bar{\nu}_\mu$ ($a_{\nu_\mu} = 6.8$, $a_{\bar{\nu}_\mu} = 3.1$,

$b_{\nu_\mu} = 0.51$, $b_{\bar{\nu}_\mu} = 0.67$) and the B_F are the branching ratios for SS^\dagger annihilations to gauge boson, Higgs boson and quark pairs. $\langle Nz^2 \rangle_{Fi}$ are the second-moments of the spectrum of neutrino type i from final state F scaled by the S mass squared,

$$\langle Nz^2 \rangle_{Fi} = \frac{1}{m_S^2} \int \left[\frac{dN}{dE} \right]_{Fi} E^2 dE \quad (4.2),$$

where $\left[\frac{dN}{dE} \right]_{Fi}$ is the differential energy spectrum of neutrino i at the surface of the Sun or Earth resulting from injection of particles in final state F at the centre of the Sun or Earth. For the case of annihilations in the Earth one multiplies (4.1) by 5.6×10^8 , corresponding to the ratio of the distance squared to the Sun to the radius squared of the Earth [13].

The capture rate is given by [12,14,16,17]

$$C = c \frac{\rho^{0.4}}{m_S v_{300}} \sum_N \sigma_{40}^N F_N(m_S) f_N \phi_N S_N / m_N \quad (4.3),$$

where σ_{40}^N is the S -nucleus elastic scattering cross-section in units of 10^{-40}cm^2 , $c = 5.8 \times 10^{24} \text{s}^{-1}$ for the Sun and $c = 5.7 \times 10^{15} \text{s}^{-1}$ for the Earth. The sum is over all species of nuclei N in the Earth or Sun. ϕ_N and f_N are given in Table A.1 of ref.17. S_N is a factor which takes into account the fact that the S dark matter particle must lose sufficient momentum to be captured. For S_N we have

$$S_N \approx (1 + A_N^{-1})^{-1} \quad ; \quad A_N = \frac{3}{2} \frac{m_S m_N}{(m_S - m_N)^2} \left[\frac{v_{\text{esc}}^2}{\bar{v}^2} \right] \phi_i \quad (4.4),$$

where v_{esc} is the escape velocity for the Sun or Earth (618kms^{-1} and 11kms^{-1} respectively). This has the correct behaviour for A_N large and small compared to 1 [14,16]. $F_N(m_S)$ is a factor which takes into account form factor suppression. The branching ratios B_F , corresponding to the rates for S annihilation in the limit of zero relative velocity, are directly obtained from (2.8).

The rate (4.1) assumes that the accretion of S particles by the Sun or Earth and their subsequent annihilation are in equilibrium, in which case the annihilation rate is given by $\Gamma_{\text{ann}} = C/2$. The condition for this to be true is that the age of the solar system t_\odot be large compared with the time for equilibrium to be established τ_A , which is defined below. In general C in (4.1) should be replaced by [12,16]

$$C \rightarrow C \tanh^2 \left(\frac{t_\odot}{\tau_A} \right) \quad (4.5),$$

where

$$\tau_A = 1/(CC_A)^{1/2} \quad ; \quad C_A = \langle \sigma v \rangle V_2/V_1^2 \quad (4.6).$$

$\langle \sigma v \rangle$ is the spin-averaged total annihilation cross-section times the relative velocity in the limit of zero relative velocity, which can be obtained from (2.8). The effective volumes V_j are given by

$$V_j = 6.5 \times 10^{28} (j m_S / 10 \text{ GeV})^{-3/2} \text{ cm}^3 \quad (4.7a),$$

for the Sun ^[12] and

$$V_j = 2.0 \times 10^{25} (j m_S / 10 \text{ GeV})^{-3/2} \text{ cm}^3 \quad (4.7b)$$

for the Earth ^[14].

A second assumption in obtaining (4.1) is that the capture rate is primarily due to single collisions with nuclei ("optically thin" limit). However, for the case of capture due to scattering from iron in the Earth, it has been pointed out that multiple collisions can enhance the capture rate ^[15]. The enhancement factor is given by

$$\alpha(\tau) = \frac{\exp(\tau_{\text{eff}} - 1)}{\tau_{\text{eff}}} \quad , \quad \tau_{\text{eff}} = \tau \beta_- \quad , \quad (4.8)$$

where

$$\tau \approx \sigma_{S-Fe} / (2.3 \times 10^{-33} \text{ cm}^2)$$

is the optical depth of the Earth, $\beta_- = 4m_S m_{Fe} / (m_S - m_{Fe})^2$, and τ_{eff} is the effective optical depth of the Earth taking into account multiple collisions. This expression is valid so long as $\text{Max}(1, \ln \beta_-) \lesssim 6/\tau_{\text{eff}}$ and $\beta_- \lesssim 20$; otherwise the enhancement must be evaluated numerically, although the largest enhancement occurs typically for $\beta_- \approx 20$ ^[15]. We have included $\alpha(\tau)$ from (4.8) in our calculations over the range where it is valid (and where enhancement is expected to be most important), in order to indicate the importance or otherwise of multiple collisions. In practice, we find that no enhancement of the event rate in detectors occurs over the range of parameters we are considering.

The $\langle N z^2 \rangle_{Fi}$ are related to the muon neutrino and anti-neutrino energy spectra coming from annihilation of S in the Sun and Earth, including in the case of the Sun the effects of the interactions of the annihilation products and neutrinos with the solar

medium^[13]. For $m_S > m_W$ the dominant contributions to the $\langle Nz^2 \rangle_{Fi}$ are from annihilation to gauge boson and t quark final states, while for $m_S < m_W$ the dominant final states contributing to $\langle Nz^2 \rangle_{Fi}$ are b quark pairs and possibly Higgs boson pairs if $m_h < m_W$. In the Appendix we discuss the values of $\langle Nz^2 \rangle_{Fi}$ coming from the different final states.

In order to calculate the capture rate for the case of the Earth one can simply use (4.3), since in this case the form factor suppression is small for most values of m_S ^[14] and so we can take $F_N(m_S) = 1$ ^[16]. [Capture is dominated by low momentum transfer scattering except for m_S close to the mass of the scattering nucleus, in which case the form factor suppression can be more significant (a factor of 0.72 for the case where $m_S = m_{Fe}$ ^[14]).] For the case of capture by the Sun, form factor suppression cannot be neglected, making the calculation of the capture rate more complicated. A simple expression for the capture rate in this case has been given by Kamionkowski^[16], which is accurate to 5% for dark matter particle masses greater than a few GeV and less than a few TeV (see also Ref.[14]). In terms of σ_{S-N} this may be written as

$$C = \frac{\pi (m_S + m_N)^2}{4 m_S^2 m_N^4} \sigma_{S-N} f_S(m_S) \quad (4.9),$$

where

$$\begin{aligned} f_S(m_S) = & 2.04 \times 10^{38} \exp[-0.0172(m_S - 10)], & m_S \leq 80 \text{ GeV} \\ & 6.10 \times 10^{37} (m_S/80)^{-1.06-0.38[(m_S-80)/920]^{1/2}}, & 80 \text{ GeV} \leq m_S \leq 1000 \text{ GeV} \\ & 1.72 \times 10^{36} (m_S/1000)^{-1.88}, & m_S \geq 1000 \text{ GeV} \end{aligned} \quad (4.10).$$

Here C is in s^{-1} and all masses are in GeV.

In Figures 4(a)-4(c) we show the results for S annihilations in the Sun for the cases $m_h = 60\text{GeV}$, 100GeV and 300GeV respectively, and in Figures 5(a)-5(c) we show the corresponding results for the case of annihilations in the Earth. Comparing Figures 4 and 5, we see that for an upper bound on Γ_{detector} corresponding to the IMB upper bound^[26], $\Gamma_{\text{detector}} < 2.65 \times 10^{-2} \text{m}^{-2} \text{yr}^{-1}$ (curve (a) in Figures 4 and 5), the strongest constraints on the parameter space come from Earth S annihilations, while for upper bounds less than around $10^{-3} \text{m}^2 \text{yr}^{-1}$ the solar S annihilations become more important. Thus we will compare the thermal relic parameter space with the Earth S annihilation

constraints for the case of the present IMB upper bound and with the solar annihilation S constraints for the case of the bounds expected from future neutrino detectors.

From Figure 5(a), corresponding to Earth S annihilations with $m_h = 60\text{GeV}$, we see that at present the IMB constraints can exclude only a small region of the thermal relic parameter space (corresponding to the iron 'resonance' at $m_S \approx 56\text{GeV}$). From Figure 4(a), we see that for an upper bound on Γ_{detector} of $10^{-3}\text{m}^{-2}\text{yr}^{-1}$, upward-moving muons from solar S annihilations can exclude a small region of the thermal relic parameter space corresponding to $\lambda_S \gtrsim 0.1$ and $m_S \lesssim 50\text{GeV}$. [We see from Figure 5(a) that for this case the bounds due to neutrinos from the Earth are stronger than those due to solar neutrinos for m_S between 20 and 80 GeV, and can probe a significant region of the thermal relic parameter space for m_S between 50 and 70 GeV.] With an upper bound $\Gamma_{\text{detector}} < 10^{-4}\text{m}^{-2}\text{yr}^{-1}$, most of the thermal relic parameter space in Figure 4(a) corresponding to $\Omega_S h^2 \lesssim 0.25$ for $m_S \lesssim 400\text{GeV}$ and a significant region of the thermal relic parameter space corresponding to a critical S density for $m_S \lesssim 50\text{GeV}$ can be investigated, while an upper bound $\Gamma_{\text{detector}} < 10^{-5}\text{m}^{-2}\text{yr}^{-1}$ would probe the whole thermal relic parameter space up to $m_S \approx 500\text{GeV}$. For larger m_h , the conclusions for $m_S \lesssim 100\text{GeV}$ are essentially unchanged, while for $m_S \gtrsim 100\text{GeV}$ the amount of thermal relic parameter space which can be investigated for a given upper bound on Γ_{detector} decreases as m_h increases.

In order to see how the IMB upper bound could be improved in the future, we can make a rough estimate of the bound which could be imposed by building neutrino detectors of larger area. The IMB bounds follow from a detector area of 400m^2 and exposure of about 1 year, corresponding to an upper bound of less than about 10 upward moving muons per year. Following ref.[27], we can estimate the area of detector required in order to achieve a given sensitivity by the area needed to detect one upward-moving muon event per year. At present, the MACRO detector at Gran Sasso, with an area $\approx 10^3\text{m}^2$, is beginning operation^[28], while a number of detectors with an effective area of order 10^4m^2 are under development (DUMAND^[29]; AMANDA^[30]; NESTOR^[31]). In addition, it has been suggested^[27] that a 1km^2 detector is needed to observe muons from neutralino dark matter in the GeV-TeV mass range, and that

this could be constructed at a cost of order 100 million U.S. dollars [32]. We see from Figure 4 that a detector of area 10^4m^2 should be able to probe the region of parameter space corresponding to curve (c), which will rule out much of the parameter space corresponding to thermal relic S dark matter with $m_S \lesssim 50\text{GeV}$. This conclusion is essentially independent of m_h , as can be seen by comparing Figures 4(a), 4(b) and 4(c). For the case of a 1km^2 detector, the area of parameter space under curve (e) in Figure 4 could in principle be searched. This would probe the entire thermal relic dark matter region for $m_S \lesssim 1.5\text{TeV}$ (500GeV , 100GeV) for the case of $m_h = 60\text{GeV}$ (100GeV , 300GeV). Thus in general the thermal relic dark matter parameter space can be probed for m_S at least up to 100GeV .

We therefore conclude that at present the IMB upper bound on the flux of upward-moving muons can impose only a slight constraint on the possibility of thermal relic S dark matter, while many of the S dark matter possibilities with $m_S \lesssim 50\text{GeV}$ should be within the reach of experiments with an area $O(10^4)\text{m}^2$ in the not-too-distant future. In the more distant future large (1km^2) detectors should be able detect or exclude S dark matter for m_S up to at least 100GeV .

We also note that comparing the next generation of Ge detectors, which might reach scattering rates $0.1\text{kg}^{-1}\text{d}^{-1}$ (Figure 3, curve e), with the next generation of neutrino detectors, which might reach upward-moving muon rates $10^{-4}\text{m}^{-2}\text{yr}^{-1}$ (Figure 4, curve c), we see that for $m_S \gtrsim 80\text{GeV}$ the constraint from upward-moving muons are dominant, while for $m_S \lesssim 80\text{GeV}$ Ge detectors impose a stronger constraint.

Up to now we have only considered the rate of upward-moving muons in discussing constraints on the (λ_S, m_S) parameter space. The upward-moving muon flux is the most important signal for high-energy neutrinos from the point of view of future large-area neutrino detectors, which are specifically designed to detect this flux. However, in discussing the present bounds on the flux of high-energy neutrinos due to SS^\dagger annihilations, we should also consider the possibility that a high-energy electron or muon neutrino could undergo a charged current interaction within the volume of the detector^[13] ('contained event'). For the case of neutrinos from the Sun the rate of

contained events per kiloton due to electron and muon neutrinos is given by^[13]

$$\Gamma_{\text{detector}} = 3.3 \times 10^{-27} C_{m_S} \Sigma_i a_i \Sigma_F B_F \langle N_z \rangle_{F_i} \text{ kt}^{-1} \text{ yr}^{-1} \quad (4.11),$$

where i is summed over the electron and muon neutrino and anti-neutrino. In the Appendix we discuss the values of $\langle N_z \rangle_{F_i}$ coming from the various final states. In Figure 6 we show the results for S annihilations in the Sun for the cases $m_h = 60\text{GeV}$, 100GeV and 300GeV , while in Figure 7 we show the corresponding results for the case of S annihilations in the Earth. The present upper bound on the rate of electron and muon contained events in the Frejus detector is^[17,33] $\Gamma_{\text{detector}} < 6.4 \text{ kt}^{-1} \text{ yr}^{-1}$, corresponding to curve (a) in Figures 6 and 7. Comparing with the upward-moving muon bounds from Figures 4 and 5, we see that at present the contained event rate imposes constraints on the parameter space which are in general weaker than those coming from the upward-moving muon flux, although at small m_S , $m_S \lesssim 20\text{GeV}$, the constraints become similar (and slightly stronger for the case of solar neutrinos).

So far in this section and in the previous section, we have considered the case of just one S scalar. For the case of N scalars of equal mass and coupling, the density of each scalar S_i contributes a proportion $1/N$ of the total halo density. The capture rate of S dark matter in the Sun and the Earth and the rate of elastic scattering in Ge detectors are proportional to the density of S_i in the halo times the cross-section for scattering from nuclei in the Sun and Earth. Thus the contribution to the event rate in a detector is reduced by a factor $1/N$ for a given S_i . The total rate from summing over i for a given m_S and λ_S is therefore unchanged. However, for a given value of the thermal relic density, the value of λ_S for a given m_S is increased by a factor \sqrt{N} , leading to an increase in the scattering cross-section and so to an increase in the event rate in Ge detectors and in neutrino detectors by a factor N for a given thermal relic density, thus making the dark matter easier to detect.

5 Conclusions

The extension of the standard model by the addition of a gauge singlet scalar provides a canonically minimal extension of the standard model which can potentially account

for dark matter. It is important, therefore, to consider in some detail the question of the relic density of the gauge singlet scalars and their possible observable signatures. In general, present experiments based on observing elastic scattering of halo dark matter particles from Ge nuclei, and on observing upward-moving muons at the Earth's surface, coming from muon neutrinos due to dark matter particle annihilation in the Sun or the Earth, can only place very weak constraints on thermal relic S dark matter, and cannot constrain the possibility that thermal relic S dark matter could account for a critical density of dark matter ($\Omega_S = 1$). However, the next generation of cryogenic Ge detectors (which hopefully should achieve bounds on the Ge scattering rate of $0.1\text{kg}^{-1}\text{d}^{-1}$) and neutrino detectors (with an effective area 10^4m^2) will be able to investigate most of the parameter space for thermal relic S scalar dark matter with $m_S \lesssim 50\text{GeV}$, while a 1km^2 neutrino detector, as suggested in order to search for heavy neutralino dark matter, would be able to exclude thermal relic S dark matter for $m_S \lesssim 100\text{GeV}$ (as would a cryogenic Ge detector if it could achieve a sensitivity of $0.01\text{kg}^{-1}\text{d}^{-1}$). For a light Higgs mass, equal to 60GeV (100GeV), a 1km^2 detector could also exclude heavier thermal relic S dark matter up to 1.5TeV (500GeV). In general, the next generation of cryogenic detectors will be the most effective in searching for S dark matter with $m_S \lesssim 80\text{GeV}$, while for $m_S \gtrsim 80\text{GeV}$ the next generation of neutrino detectors will be most effective.

The coupling of a gauge singlet scalar to the standard model Higgs doublet is unique in form and inevitably will be a feature of many particle physics models beyond the standard model. We believe the results presented here may generally be useful in the study of such models and of their cosmological consequences.

Appendix. $\langle N_Z^2 \rangle_{F_i}$ and $\langle N_Z \rangle_{F_i}$ from SS^\dagger annihilations.

In this Appendix we give the dominant contributions to $\langle N_Z^2 \rangle_{F_i}$ and $\langle N_Z \rangle_{F_i}$ for the gauge boson, Higgs boson and quark final states coming from SS^\dagger annihilation. We will use the discussion of Ritz and Seckel ^[13] (RS) for the case of the quark final states,

while for the case of the gauge boson final states we will follow Ref.[16] and consider $\langle N_{Z^2} \rangle_{F_i}$ and $\langle N_Z \rangle_{F_i}$ to mostly originate from the highest-energy "semiprompt" W and Z decays to neutrinos. For the case of the Higgs boson final states we will adapt the results of RS to obtain $\langle N_{Z^2} \rangle_{F_i}$ and $\langle N_Z \rangle_{F_i}$.

$SS^\dagger \rightarrow WW, ZZ$

In this case the dominant contribution to $\langle N_{Z^2} \rangle_{F_{\nu_\mu}}$ comes from muon neutrinos originating in the decays $W^+ \rightarrow \mu^+ \nu_\mu$ and $Z^0 \rightarrow \nu_\mu \bar{\nu}_\mu$. The mean energy squared of the neutrinos is $E_o = \frac{m_S^2}{4}(1 + \beta^2/3)$, where β is the velocity of the decaying W or Z^[16] [$\beta = (1 - m_W^2/m_S^2)^{1/2}$ for the case of the W]. This assumes that in the rest frame of the W, the W decays isotropically to final states each of energy $m_W/2$. The branching ratio of W^+ to ν_μ decays is given by 1 divided by the number of SU(2) doublets to which W can decay, which gives 1/9 for W decaying to all lepton doublets and 1st and 2nd generation quark doublets. Thus, noting that N is the number of neutrinos produced per injected boson or fermion pair^[13], we see that the $\langle N_{Z^2} \rangle_{F_i}$ following from annihilation to W pairs can be estimated to be

$$\langle N_{Z^2} \rangle_{W \nu_\mu} \approx \frac{1}{9} \frac{1}{4} (1 + \beta^2/3) = 0.028(1 + \beta^2/3) \quad (A.1).$$

For the case of annihilation to Z pairs, the branching ratio for $Z \rightarrow \bar{\nu}_\mu \nu_\mu$ is 0.066^[19], and so the $\langle N_{Z^2} \rangle_{F_i}$ can be estimated to be

$$\langle N_{Z^2} \rangle_{Z \nu_\mu} \approx 2(0.066) \frac{1}{4} (1 + \beta^2/3) = 0.033(1 + \beta^2/3) \quad (A.2),$$

where the factor 2 occurs because either of the Z's produced by S annihilation can lead to a ν_μ . The same results are obtained for $i = \bar{\nu}_\mu$. For the case of the $\langle N_Z \rangle_{F_i}$ one obtains in the same way, for $i = e$ and μ ,

$$\langle N_Z \rangle_{W \nu_i} \approx \frac{1}{9} \frac{1}{2} = 0.056 \quad (A.3)$$

and

$$\langle N_Z \rangle_{Z \nu_i} \approx 2(0.066) \frac{1}{2} = 0.066 \quad (A.4),$$

where we have replaced the mean squared energy of the neutrinos $\frac{m_S^2}{4}(1 + \beta^2/3)$ in (A.1) and (A.2) by the mean squared energy in the rest frame $m_S/2$. The values of $\langle Nz \rangle_{Fi}$ for $\bar{\nu}_i$ are equal to those of ν_i .

These results are true for the case where interactions of the W, Z and neutrinos with the Sun or Earth are ignored. This is justified for the Earth, but for the case of the Sun there is an additional suppression factor due to the absorption of muon neutrinos (due to charged current interactions) and loss of neutrino energy (due to neutral current interactions) as the neutrinos pass through the Sun^[13]. (The W and Z will decay fast enough that the effect of their interaction with the solar medium prior to their decay can be ignored^[13].) The suppression factors are given by^[13]

$$P_i = 1/(1 + E_o\tau_i)^{n+\alpha_i} \quad (A.5),$$

where E_o is the initial neutrino energy and $n = 2(1)$ for the case of $\langle Nz^2 \rangle_{Fi}$ ($\langle Nz \rangle_{Fi}$). $\alpha_{\nu_\mu} = 5.1$, $\alpha_{\bar{\nu}_\mu} = 9.0$, $\tau_{\nu_\mu} = 1.01 \times 10^{-3} \text{GeV}^{-1}$ and $\tau_{\bar{\nu}_\mu} = 3.8 \times 10^{-4} \text{GeV}^{-1}$ for $i = e, \mu$. The unsuppressed $\langle Nz^2 \rangle_{Fi}$ and $\langle Nz \rangle_{Fi}$ are multiplied by the P_i in order to obtain the true $\langle Nz^2 \rangle_{Fi}$ and $\langle Nz \rangle_{Fi}$ for the case of neutrinos from the Sun.

It is important to note that the assumption that the $\langle Nz^2 \rangle_{Fi}$ and $\langle Nz \rangle_{Fi}$ are dominated by the "semiprompt" decays of the W and Z is well justified for the case of the unsuppressed $\langle Nz^2 \rangle_{Fi}$ and $\langle Nz \rangle_{Fi}$ ^[16], which is appropriate for the case of neutrinos from the Earth. However, for the case of neutrinos from the Sun, because the higher-energy neutrinos from semiprompt decays are preferentially absorbed relative to the lower-energy neutrinos coming from secondary decays^[13] (such as W's decaying to pairs of quarks which subsequently decay to neutrinos), the secondary decay neutrinos may become important at large S masses. At the end of this Appendix we make an estimate of the importance of the secondary decays for the case of the Z boson final state, where it is shown that the primary decays dominate $\langle Nz^2 \rangle_{F\nu}$ ($\langle Nz^2 \rangle_{F\bar{\nu}}$) for m_S up to at least 1.4 TeV (2.2 TeV), and up to at least 860 GeV (1.3 TeV) for $\langle Nz \rangle_{F\nu}$ ($\langle Nz \rangle_{F\bar{\nu}}$). From the Figures we see that an underestimate of the $\langle Nz^2 \rangle_{Fi}$ or $\langle Nz \rangle_{Fi}$ by a factor of 2 will make very little difference to our conclusions. Thus we expect that in general our results for the case of solar S

annihilations will be reliable for m_S up to at least ~ 1.5 TeV for the upward-moving muons and up to at least ~ 1 TeV for the contained events.

$$\mathbf{SS}^\dagger \rightarrow \bar{\mathbf{t}}\mathbf{t} \ , \ \bar{\mathbf{b}}\mathbf{b}$$

In the case of quark final states, one must consider the details of hadronization and fragmentation of the final state quarks, which will produce hadron jets. RS ^[13] have used the results of the Lund Monte Carlo program, which simulates the final states of e^+ , e^- annihilations into fermion pairs, in order to calculate the values of $\langle Nz^2 \rangle_{Fi}$ and $\langle Nz \rangle_{Fi}$ due to dark matter particles annihilating to fermion pairs. For the case of non-interacting final state quarks (appropriate for S annihilations in the Earth), one can use the RS results directly. In general, the $\langle Nz^2 \rangle_{Fi}$ and $\langle Nz \rangle_{Fi}$ are given by ^[13]

$$\langle Nz^2 \rangle_{Fi} = \frac{N}{3} \langle y^2 \rangle \left(\langle z_F^2 \rangle - \frac{1}{4} z_M^2 \right) \quad (\text{A.6})$$

and

$$\langle Nz \rangle_{Fi} = \frac{N}{2} \langle y \rangle \langle z_F \rangle \quad (\text{A.7}),$$

where $z_M^2 = m_H^2/m_S^2$, N , $\langle y^n \rangle$, the hadron mass m_H , and $\langle z_F^n \rangle$ are given in Tables 2 and 3 of Ref. [13]. In this we have assumed that the mean hadron energy (scaled by the S mass) when the hadron decays, $\langle z_H \rangle$, is equal to the hadron energy after fragmentation $\langle z_F \rangle$, which is true if the hadrons are not slowed by the astrophysical medium (Sun or Earth) before they decay. We will show below that this is in general justified for the case of interest to us here. One has to correct (A6) and (A7) for the case of m_S near the threshold for producing a hadron, since in this case energy conservation implies $\langle z_F \rangle \rightarrow 1$. RS make the replacement $\langle z_F^n \rangle \rightarrow \langle z_F^n \rangle + (1 - \langle z_F^n \rangle) z_M^n$ in order to take this into account ^[13]. Using (A6) and (A7) (corrected for thresholds) and the results of Ref. [13] we obtain, for the $\bar{t}t$ final state,

$$\langle Nz^2 \rangle_{t\nu_\mu} = 1.7 \times 10^{-2} (1 - 0.04 z_M^2) \quad (\text{A.8})$$

and

$$\langle Nz \rangle_{t\nu_i} = 4.7 \times 10^{-2} (1 + 0.41 z_M^2) \quad (\text{A.9}),$$

where $i = e$ or μ . The same results are obtained for the antineutrinos. For the $\bar{b}b$ final state we obtain

$$\langle Nz^2 \rangle_{b\nu_\mu} = 6.5 \times 10^{-3}(1 + 0.39z_M^2) \quad (\text{A.10})$$

and

$$\langle Nz \rangle_{b\nu_i} = 2.8 \times 10^{-2}(1 + 0.41z_M^2) \quad (\text{A.11}).$$

These results are for the case where the interactions with the astrophysical medium are ignored. For the case of solar annihilations one has to consider the possible effects of hadrons slowing before they decay, as well as the effect of neutrinos losing energy or being absorbed as they pass through the Sun. In fact, we can ignore the effect of hadrons slowing for the case of interest to us here. For the b quark final state, the effect of slowing is only important for $E_b > E_b^c = 470\text{GeV}$ [13]. But the b quark final state is important only when the W and Z final states are kinematically disallowed, $m_S < m_W$, in which case we can ignore the slowing of the hadrons. For the case of the t quarks, one has $E_t^c = (m_t/m_b)^{1/2}E_b^c = 2.3\text{TeV}$ for $m_t = 120\text{GeV}$. For m_S large compared with m_W , the branching ration to the W final state is much larger than that to the t quark final state. [From (2.8) we find $B_{WW}/B_{tt} \approx 2m_S^2/3m_t^2$ in the limit of large m_S .] Thus we see that for values of m_S for which the slowing of t quarks becomes important (greater than 1 TeV), we can ignore the t quark final states. Therefore in general we can ignore the effect of quarks slowing before they decay.

In order to take account of the interaction of the neutrinos with the Sun, we use the method of RS. We simply integrate the differential energy spectrum, including the P_i factors from (A.5):

$$\langle Nz^n \rangle_{FiA} = \int \left[\frac{dN}{dz} \right]_{Fi} \frac{z^n dz}{(1 + z/z_{Si})^{n+\alpha_i}} \quad (\text{A.12}),$$

where $z_{Si} = 1/\tau_i m_S$ and $\langle Nz^n \rangle_{FiA}$ is the moment of the neutrino distribution including the effect of interactions with the Sun. For $(n + \alpha_i)z/z_{Si}$ small compared with 1, the denominator can be expanded to give

$$\langle Nz^n \rangle_{FiA} = \langle Nz^n \rangle_{Fi} \left[1 - \frac{\langle z^{n+1} \rangle}{\langle z^n \rangle} \frac{n + \alpha_i}{z_{Si}} \right] \quad (\text{A.13}).$$

Using Table 3 and Eq.(32) of Ref.[13] we find that $(\langle z \rangle, \langle z^2 \rangle, \langle z^3 \rangle)$ equals $(0.13, 4.4 \times 10^{-2}, 2.1 \times 10^{-2})$ for the t quark final state and $(0.13, 2.9 \times 10^{-2}, 9.5 \times 10^{-3})$

for the b quark final state. Thus we obtain, for the case of the t quark final state,

$$\langle N_{Z^2} \rangle_{t\nu_\mu A} = \langle N_{Z^2} \rangle_{t\nu_\mu} [1 - m_S/(290 \text{ GeV})] \quad (\text{A.14}),$$

$$\langle N_{Z^2} \rangle_{t\bar{\nu}_\mu A} = \langle N_{Z^2} \rangle_{t\bar{\nu}_\mu} [1 - m_S/(492 \text{ GeV})] \quad (\text{A.15}),$$

$$\langle N_Z \rangle_{t\nu_\mu A} = \langle N_Z \rangle_{t\nu_\mu} [1 - m_S/(478 \text{ GeV})] \quad (\text{A.16}),$$

$$\langle N_Z \rangle_{t\bar{\nu}_\mu A} = \langle N_Z \rangle_{t\bar{\nu}_\mu} [1 - m_S/(765 \text{ GeV})] \quad (\text{A.17}),$$

and, for the b final state,

$$\langle N_{Z^2} \rangle_{b\nu_\mu A} = \langle N_{Z^2} \rangle_{b\nu_\mu} [1 - m_S/(422 \text{ GeV})] \quad (\text{A.18}),$$

$$\langle N_{Z^2} \rangle_{b\bar{\nu}_\mu A} = \langle N_{Z^2} \rangle_{b\bar{\nu}_\mu} [1 - m_S/(716 \text{ GeV})] \quad (\text{A.19}),$$

$$\langle N_Z \rangle_{b\nu_\mu A} = \langle N_Z \rangle_{b\nu_\mu} [1 - m_S/(740 \text{ GeV})] \quad (\text{A.20}),$$

$$\langle N_Z \rangle_{b\bar{\nu}_\mu A} = \langle N_Z \rangle_{b\bar{\nu}_\mu} [1 - m_S/(1200 \text{ GeV})] \quad (\text{A.21}).$$

These should be accurate so long as the suppression factors are not too small compared with 1. However, for the case of the t quark we see that for $\langle N_{Z^2} \rangle_{t\nu_\mu A}$ the approximation breaks down for m_S larger than about 250 GeV. In this case an alternative method for estimating the suppression of neutrinos must be used. From Table 3 of Ref.[13] we see that the effect of fragmentation of the t quark is quite small, with $\langle z_F \rangle = 0.87$ and $\langle z_F^2 \rangle = 0.78$, compared with 1 for the case without fragmentation. In addition, most of the neutrinos come from the primary decay mode to neutrinos, $t \rightarrow b\mu^+\nu_\mu$ [13]. This can be seen by comparing the naive estimate based on this decay mode with the results of (A.8) and (A.9). Assuming that in the rest frame of the decaying quark the decay is isotropic with each decay product having energy $\approx m_t/3$, the energy squared of the neutrino is $(m_S^2/9)(1 + \beta^2/3)$, where $\beta = (1 - m_t^2/m_S^2)^{1/2}$. The branching ration for this decay is 1/9. Thus we obtain

$$\langle N_{Z^2} \rangle_{t\nu_\mu} \approx \left(\frac{1}{9}\right)^2 (1 + \beta^2/3) = 0.012(1 + \beta^2/3) \quad (\text{A.22}),$$

and

$$\langle N_Z \rangle_{t\nu_\mu} \approx \frac{1}{9} \frac{1}{3} = 0.037 \quad (\text{A.23}),$$

which in the limit $\beta \rightarrow 1$ are close to (A.8) and (A.9).

Thus in this case a reasonable approximation to the suppression factors is to use the P_i with $E_o = m_t/3$. At large values of m_S , where such an approach may fail (due to the preferential stopping of the higher-energy primary decay neutrinos, such that the spectrum is not dominated by these neutrinos ^[13]), the t quark final state can be neglected compared with the gauge boson final state when calculating event rates. Thus we will use (A.18) - (A.21) for the b quark final state and the P_i suppression factors for the t quark final state.

$$\mathbf{SS}^\dagger \rightarrow \mathbf{h}^o \mathbf{h}^o$$

RS do not explicitly discuss this case. However, we can easily adapt their results. The main decay mode of the Higgs boson when $m_h < m_W$ (with branching ratio ≈ 0.9) is to $\bar{b}b$ pairs. (The Higgs boson final state can in general be neglected compared with the gauge boson final states when these are kinematically allowed.) The neutrinos occur in the decay of these $\bar{b}b$ pairs. We can simply regard the decay of the $h^o h^o$ pair as the injection of two $\bar{b}b$ pairs, with each b quark having a mean energy $m_S/2$. This should be a good approximation for $m_S/2 \gg m_b$. In this case we can use the RS results for $\bar{b}b$ pairs, but with $m_S \rightarrow m_S/2$ and an overall factor of 2. This gives, for the non-interacting case,

$$\langle N Z^2 \rangle_{h^o \nu_\mu} = 3.3 \times 10^{-3} (1 + 1.6 z_M^2) \quad (\text{A.24})$$

and

$$\langle N z \rangle_{h^o \nu_i} = 2.8 \times 10^{-2} (1 + 0.82 z_M^2) \quad (\text{A.11}).$$

The suppression factors for the interacting case are $[1 - m_S/(844\text{GeV})]$ (ν) and $[1 - m_S/(1.4\text{TeV})]$ ($\bar{\nu}$) for the $\langle N Z^2 \rangle_{F_i}$ and $[1 - m_S/(1.5\text{TeV})]$ (ν) and $[1 - m_S/(2.4\text{TeV})]$ ($\bar{\nu}$) for the $\langle N z \rangle_{F_i}$.

We can also use this method to estimate the contribution of the secondary decay neutrinos to the $\langle N Z^2 \rangle_{F_i}$ and $\langle N z \rangle_{F_i}$ for the case of solar S annihilations to gauge boson final states. For the case of S annihilations to a pair of Z bosons, the secondary neutrinos come from the decay of the Z 's to a $\bar{b}b$, $\bar{c}c$, or $\bar{\tau}\tau$ pair. (Other lighter quarks or leptons are stopped in the Sun prior to their decay and can be neglected ^[13].) Thus

we can use the results of RS for the case of injection of a pair of b or c quarks or τ leptons each of energy $m_S/2$. (For the b or c quarks, this will overestimate the contribution when $m_S/2 > E_b^c$ or E_c^c , since we are then neglecting the slowing of the b and c quarks prior to their decay.) The branching ration for Z decay is 0.15 to a b quark pair, 0.12 to a c quark pair, and 0.033 to a τ lepton pair ^[19]. Thus we find, using the results of RS, that the contribution of the secondary decays is given by

$$\langle N_{Z^2} \rangle_{Zb\nu} \approx 4.9 \times 10^{-4} \quad (A.26a),$$

$$\langle N_{Z^2} \rangle_{Zc\nu} \approx 1.7 \times 10^{-4} \quad (A.26b),$$

$$\langle N_{Z^2} \rangle_{Z\tau\nu} \approx 3.8 \times 10^{-4} \quad (A.26c),$$

and

$$\langle N_Z \rangle_{Zb\nu} \approx 4.2 \times 10^{-3} \quad (A.27a),$$

$$\langle N_Z \rangle_{Zc\nu} \approx 1.4 \times 10^{-3} \quad (A.27b),$$

$$\langle N_Z \rangle_{Z\tau\nu} \approx 1.7 \times 10^{-3} \quad (A.27c),$$

where, for example, $\langle N_{Z^2} \rangle_{Zb\nu}$ denotes the unsuppressed contribution coming from Z decays to b quark pairs. Comparing with the primary Z decays, we find that the unsuppressed primary decay contribution to $\langle N_{Z^2} \rangle_{F_i}$ is about 45 times the secondary contribution, and that the unsuppressed primary decay contribution to $\langle N_Z \rangle_{F_i}$ is about nine times the secondary contribution. Thus, ignoring suppression of the secondary neutrinos, we find from (A.5) that the primary and secondary decay neutrino contributions become comparable at $m_S \approx 1.4\text{TeV}$ for $\langle N_{Z^2} \rangle_{Z\nu}$, $m_S \approx 2.2\text{TeV}$ for $\langle N_{Z^2} \rangle_{Z\bar{\nu}}$, $m_S \approx 860\text{TeV}$ for $\langle N_Z \rangle_{Z\nu}$, and $m_S \approx 1.3\text{TeV}$ for $\langle N_Z \rangle_{Z\bar{\nu}}$.

References

- [1] E.W.Kolb and M.S.Turner, *The Early Universe*, (Addison-Wesley, Reading MA, 1990).
- [2] A.Dekel, S.M.Faber and M.Davis, in 'From the Planck Scale to the Weak Scale', *Proceedings, Santa Cruz, California, 1987*, edited by H.Haber (World Scientific, Singapore, 1987), Vol.2.
- M.S.Turner, 'Dark Matter in the Universe', Fermilab preprint FERMILAB-Conf-91/78-A.
- [3] J.Yang, M.S.Turner, G.Steigman, D.N.Schramm and K.A.Olive, *Astrophys.J.* 281 (1984) 493
- K.A.Olive, D.N.Schramm, G.Steigman and T.P.Walker, *Phys.Lett.* 236B (1990) 454
- T.P.Walker, G.Steigman, D.N.Schramm, K.A.Olive and H.S.Kang, *Astrophys.J.* 376 (1991) 51.
- [4] A.Guth, *Phys.Rev.D*23 (1981) 347.
- [5] G.R.Blumental, S.M.Faber, J.R.Primack and M.Rees, *Nature* 311 (1984) 517.
- [6] G.F.Smoot et al, *Astrophys.J.* 396 (1992) L1; E.L.Wright et al, *ibid.* 396 (1992) L13.
- [7] D.Hegyi and K.A.Olive, *Phys.Lett.* 126B (1983) 28; *Astrophys.J.* 303 (1986) 56.
- D.Ryu, K.A.Olive and J.Silk, *Astrophys.J.* 353 (1990) 81.
- [8] D.Richstone, A.Gould, P.Guhathakurta and C.Flynn, *Astrophys. J.* 388 (1992) 354.
- H.B.Richer and G.G.Fahlman, *Nature* 358 (1992) 383.
- [9] C.Alcock et al., *Nature* 365 (1993) 621.
- E.Aubourg et al., *Nature* 365 (1993) 623.
- [10] S.P.Ahlen et al, *Phys.Lett.* 195B (1987) 603
- D.O.Caldwell et al, *Phys.Rev.Lett.* 61 (1988) 510; *Phys.Rev.Lett.* 65 (1990) 1305.
- [11] D.O.Caldwell, *Nucl.Phys.B (Proc.Suppl.)* 31 (1983) 371.
- [12] W.H.Press and D.Spergel, *Astrophys.J.* 296 (1985) 679.
- K.Greist and D.Seckel, *Nucl.Phys.* B283 (1987) 681; B296 (1988) 1034(E).

- [13] S.Ritz and D.Seckel, Nucl.Phys. B304 (1988) 877.
- [14] A.Gould, Astrophys.J. 321 (1987) 571; 368 (1991) 610; 388 (1992) 338.
- [15] A.Gould, Astrophys.J. 387 (1992) 21.
- [16] M.Kamionkowski, Phys.Rev. D44 (1991) 3021.
- [17] G.B.Gelmini, P.Gondolo and E.Roulet, Nucl.Phys. B351 (1991) 623.
- [18] B.W.Lee and S.Weinberg, Phys.Rev.Lett. 39 (1977) 165.
- [19] V.D.Barger and R.J.N.Phillips, Collider Physics (Addison-Wesley, Reading MA, 1987).
- [20] G.W.Anderson and L.J.Hall, Phys.Rev. D42 (1992) 2685.
- [21] M.A.Shifman, A.I.Vainstein and V.I.Zahkarov, Phys.Lett. 78B (1978) 443
T.P.Cheng, Phys.Rev. D38 (1988) 2869
H.Y.Cheng, Phys.Lett 219B (1989) 347
R.Barbieri, M.Frigeni and G.F.Giudice, Nucl.Phys. B313 (1989) 725.
- [22] J.Ellis and R.A.Flores, Phys.Lett. 263B (1991) 259.
- [23] K.Freese, J.Frieman and A.Gould, Phys.Rev. D37 (1988) 3388.
K.Greist, Phys.Rev. D38 (1988) 2357.
- [24] P.F.Smith and J.D.Lewin, Phys.Rep. 187 (1990) 203.
P.F.Smith et al, Phys.Lett. 255B (1991) 451.
- [25] B.Cabrera, Proceedings of the IFT Conference on Dark Matter, Gainesville, Florida (1992).
J.Ellis and R.A.Flores, CERN-TH-6483/92 (1992)
- [26] IMB Collaboration, J.M.LoSecco et al, Phys.Lett. 188B (1987) 388.
R.Svoboda et al, Astrophys.J. 315 (1987) 420.
- [27] F.Halzen, T.Stelzer and M.Kamionkowski, Phys.Rev. D45 (1992) 4439.
- [28] R.C.Webb, in Proceedings of the International School of Astroparticle Physics, Ed. D.V.Nanopoulos, World Scientific, Singapore (1993).
- [29] A.Okada et al, Proceedings of the Workshop on High Energy Neutrino Astrophysics, edited by V.J.Stenger et al, World Scientific, Singapore (1992)
DUMAND Collaboration, Phys.Rev. D42 (1990) 3613.
- [30] S.Tilev et al, Proceedings of the 23rd International Cosmic Ray Conference, Cal-

gary, Canada (1993).

[31] Proceedings of the NESTOR Workshop, edited by L.K.Resvanis, Univ. of Athens (1993).

[32] F.Halzen and J.G.Learned, Univ. of Wisconsin-Madison preprint MAD/PH/759 (1993).

J.G.Learned, Nucl.Phys.B (Proc.Suppl.) 31 (1993) 456.

[33] Frejus Collaboration, presented by H.J.Daum, Topical Seminar on Astrophysics and Particle Physics, San Miniato, Italy 1989.

Figure Captions

Figure 1a S annihilation to h^0 pairs.

Figure 1b S annihilation to W and Z pairs.

Figure 1c S annihilation to fermion pairs.

Figure 2a Thermal relic S scalar density (in units of $\Omega_S h^2$) as a function of λ_S and m_S (in units of GeV) for m_h equal to 60GeV.

Figure 2b Thermal relic S scalar density for m_h equal to 100GeV.

Figure 2c Thermal relic S scalar density for m_h equal to 300GeV.

Figure 2d Thermal relic S scalar density for m_h equal to 500GeV.

Figure 3a Ge scattering rate for the case $m_h = 60\text{GeV}$. The contours correspond to $\sigma_{S-\text{Ge}} =$ a) $1000\text{kg}^{-1}\text{d}^{-1}$, b) $100\text{kg}^{-1}\text{d}^{-1}$, c) $10\text{kg}^{-1}\text{d}^{-1}$, d) $1\text{kg}^{-1}\text{d}^{-1}$, e) $0.1\text{kg}^{-1}\text{d}^{-1}$ and f) $0.01\text{kg}^{-1}\text{d}^{-1}$.

Figure 3b Ge scattering rate for the case $m_h = 100\text{GeV}$.

Figure 3c Ge scattering rate for the case $m_h = 300\text{GeV}$.

Figure 4a Rate of upward-moving muons at the Earth's surface due to neutrinos from S annihilation in the Sun, for the case $m_h = 60\text{GeV}$. The contours correspond to $\Gamma_{\text{detector}} =$ a) $2.65 \times 10^{-2}\text{m}^{-2}\text{yr}^{-1}$, b) $10^{-3}\text{m}^{-2}\text{yr}^{-1}$, c) $10^{-4}\text{m}^{-2}\text{yr}^{-1}$, d) $10^{-5}\text{m}^{-2}\text{yr}^{-1}$ and e) $10^{-6}\text{m}^{-2}\text{yr}^{-1}$.

Figure 4b Rate of upward-moving muons at the Earth's surface due to neutrinos from S annihilation in the Sun, for the case $m_h = 100\text{GeV}$.

Figure 4c Rate of upward-moving muons at the Earth's surface due to neutrinos from S annihilation in the Sun, for the case $m_h = 300\text{GeV}$.

Figure 5a Rate of upward-moving muons at the Earth's surface due to neutrinos from S annihilation in the Earth, for the case $m_h = 60\text{GeV}$. The contours correspond to $\Gamma_{\text{detector}} =$ a) $2.65 \times 10^{-2} \text{m}^{-2} \text{yr}^{-1}$, b) $10^{-3} \text{m}^{-2} \text{yr}^{-1}$, c) $10^{-4} \text{m}^{-2} \text{yr}^{-1}$, d) $10^{-6} \text{m}^{-2} \text{yr}^{-1}$.

Figure 5b Rate of upward-moving muons at the Earth's surface due to neutrinos from S annihilation in the Earth, for the case $m_h = 100\text{GeV}$.

Figure 5c Rate of upward-moving muons at the Earth's surface due to neutrinos from S annihilation in the Earth, for the case $m_h = 300\text{GeV}$.

Figure 6a Rate of contained events due to neutrinos from S annihilation in the Sun, for the case $m_h = 60\text{GeV}$. The contours correspond to $\Gamma_{\text{detector}} =$ a) $6.4 \text{kt}^{-1} \text{yr}^{-1}$, b) $1 \text{kt}^{-1} \text{yr}^{-1}$, c) $0.1 \text{kt}^{-1} \text{yr}^{-1}$, d) $10^{-2} \text{kt}^{-1} \text{yr}^{-1}$ and e) $10^{-3} \text{kt}^{-1} \text{yr}^{-1}$.

Figure 6b Rate of contained events due to neutrinos from S annihilation in the Sun, for the case $m_h = 100\text{GeV}$.

Figure 7a Rate of contained events due to neutrinos from S annihilation in the Earth, for the case $m_h = 60\text{GeV}$. The contours correspond to $\Gamma_{\text{detector}} =$ a) $6.4 \text{kt}^{-1} \text{yr}^{-1}$, b) $1 \text{kt}^{-1} \text{yr}^{-1}$, c) $0.1 \text{kt}^{-1} \text{yr}^{-1}$, d) $10^{-2} \text{kt}^{-1} \text{yr}^{-1}$ and e) $10^{-3} \text{kt}^{-1} \text{yr}^{-1}$.

Figure 7b Rate of contained events due to neutrinos from S annihilation in the Earth, for the case $m_h = 100\text{GeV}$.

Fig 1

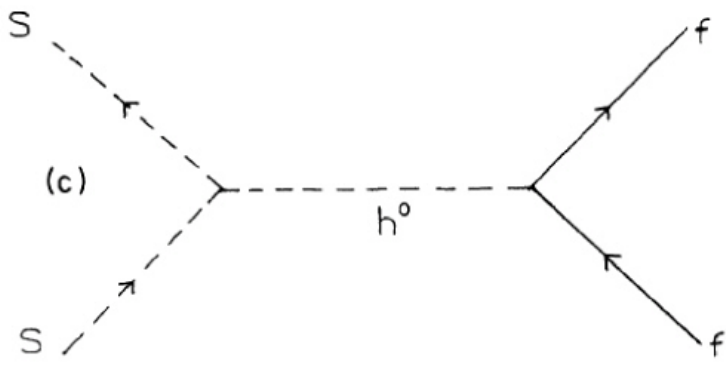
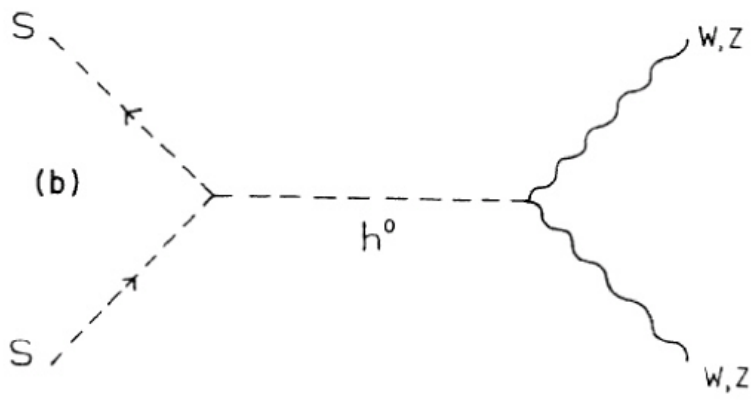
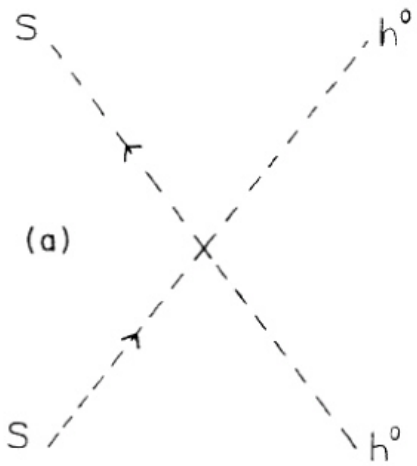


Fig 2

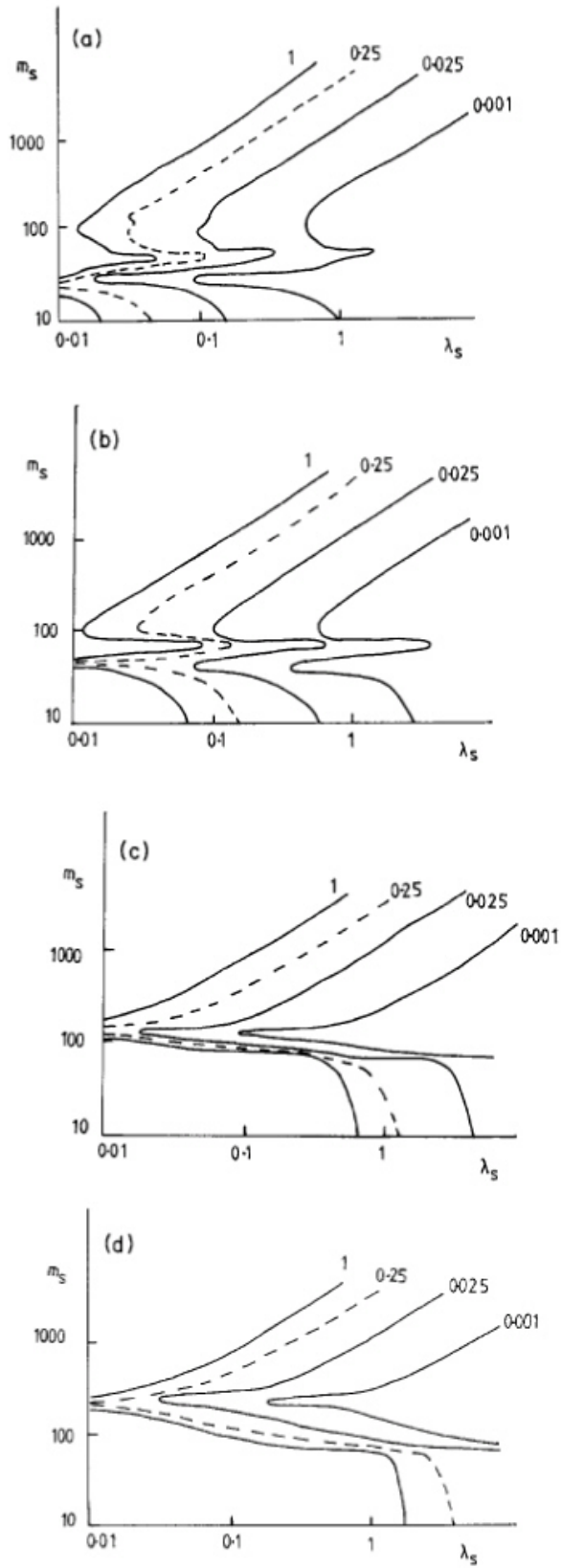


Fig.3

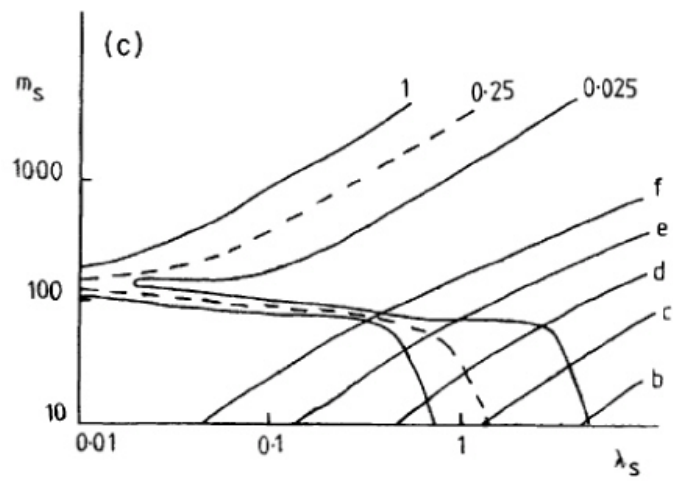
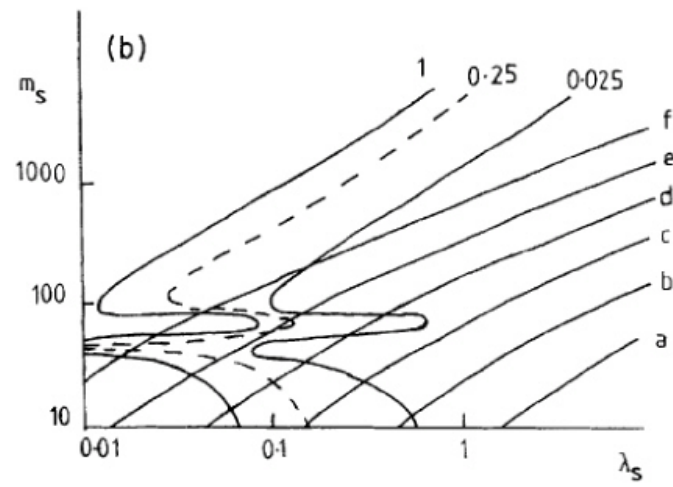
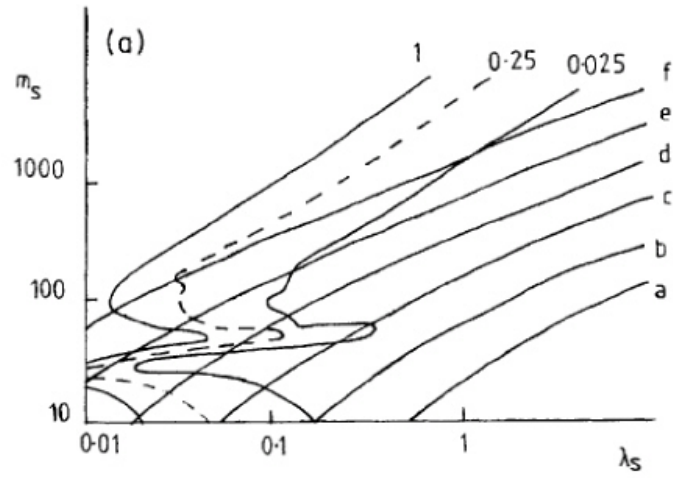


Fig.4

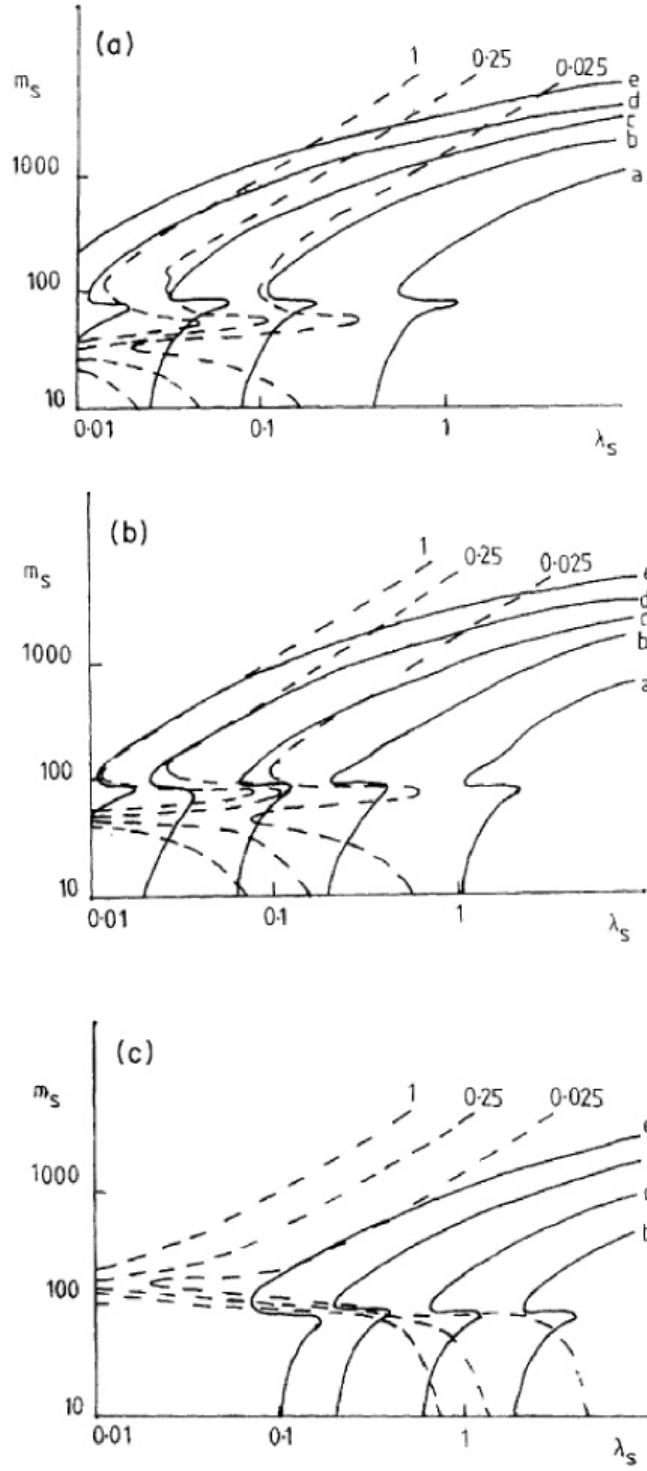


Fig.5

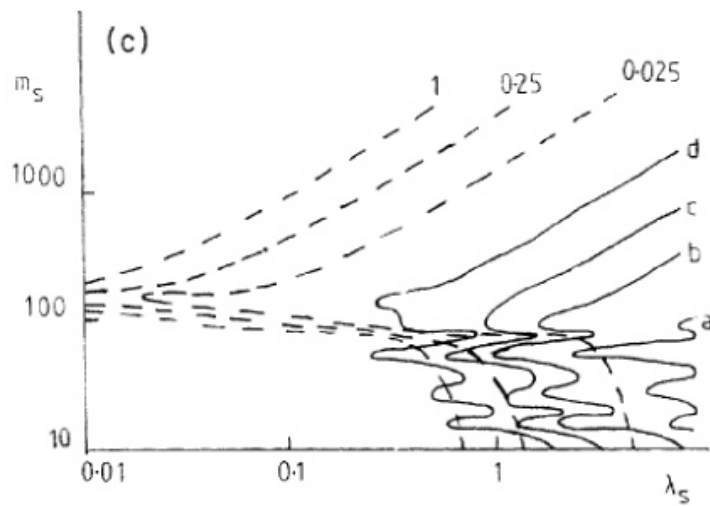
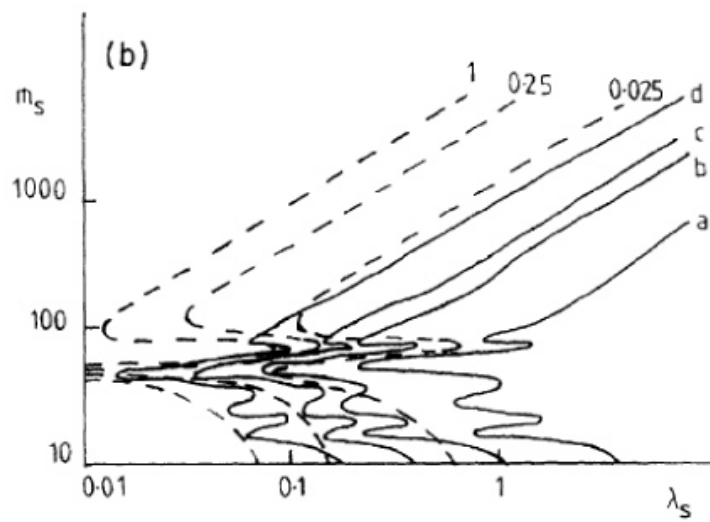
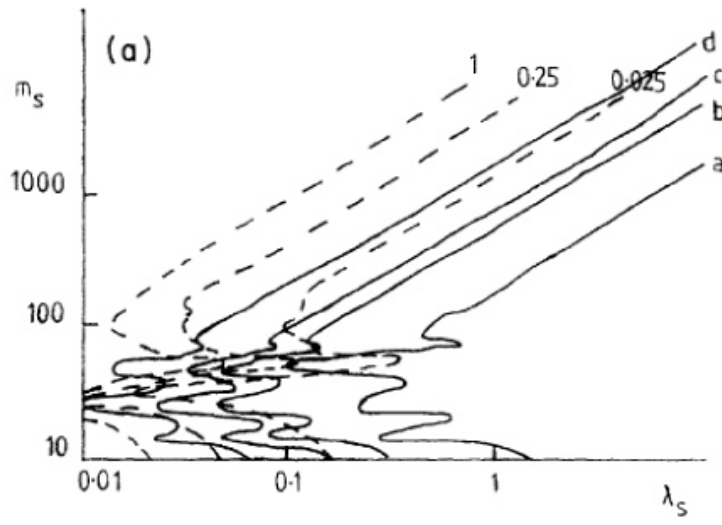


Fig. 6(a)

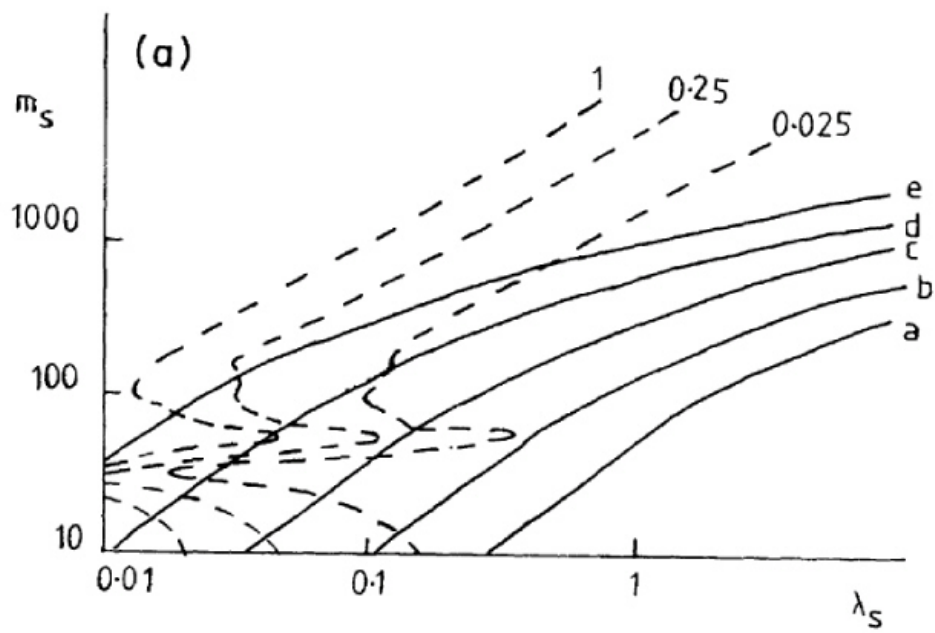


Fig. 6(b)

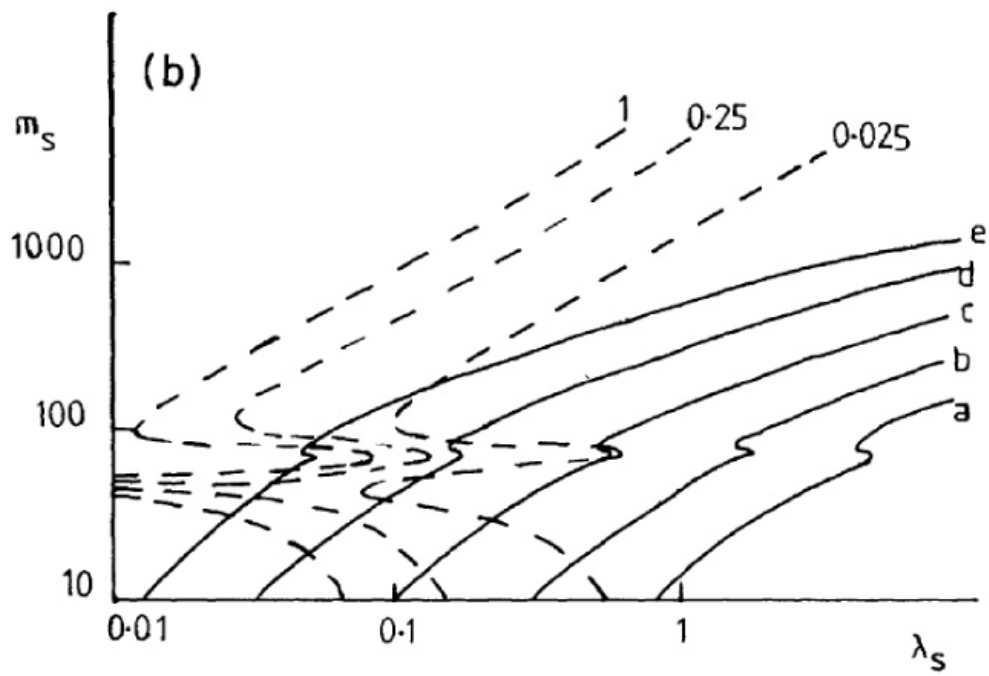


Fig. 7(a)

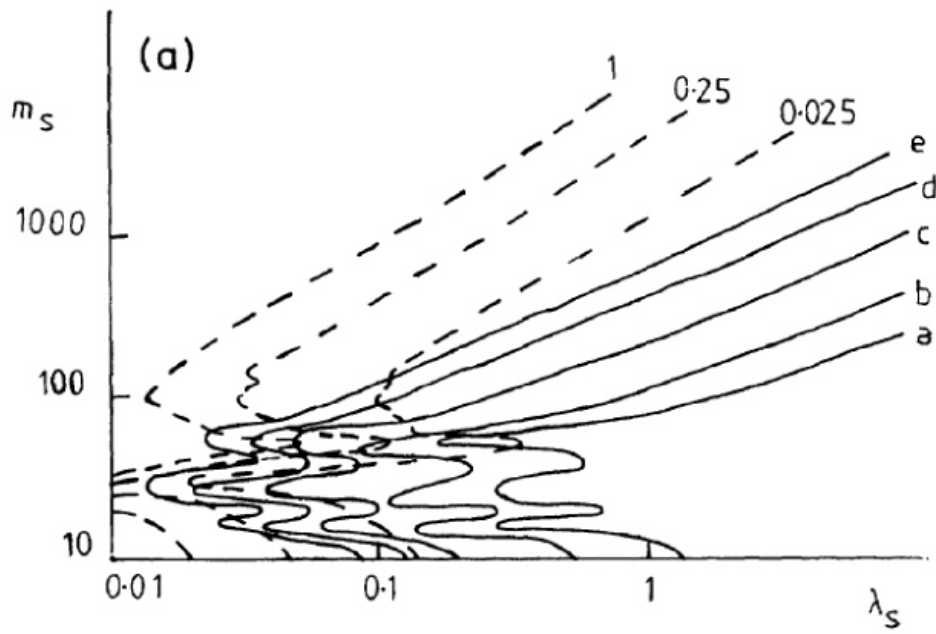


Fig. 7(b)

